B_1 Mapping for Bias-Correction in Quantitative T_1 Imaging of the Brain at 3T Using Standard Pulse Sequences

Mathieu Boudreau, MSc,[1]* Christine L. Tardif, PhD,[2] Nikola Stikov, PhD,[3,4] John G. Sled, PhD,[5,6] Wayne Lee, MSc,[6] and G. Bruce Pike, PhD[1,7]

Purpose: B_1 mapping is important for many quantitative imaging protocols, particularly those that include whole-brain T_1 mapping using the variable flip angle (VFA) technique. However, B_1 mapping sequences are not typically available on many magnetic resonance imaging (MRI) scanners. The aim of this work was to demonstrate that B_1 mapping implemented using standard scanner product pulse sequences can produce B_1 (and VFA T_1) maps comparable in quality and acquisition time to advanced techniques.

Materials and Methods: Six healthy subjects were scanned at 3.0T. An interleaved multislice spin-echo echo planar imaging double-angle (EPI-DA) B_1 mapping protocol, using a standard product pulse sequence, was compared to two alternative methods (actual flip angle imaging, AFI, and Bloch-Siegert shift, BS). Single-slice spin-echo DA B_1 maps were used as a reference for comparison (Ref. DA). VFA flip angles were scaled using each B_1 map prior to fitting T_1; the nominal flip angle case was also compared.

Results: The pooled-subject voxelwise correlation (ρ) for B_1 maps (BS/AFI/EPI-DA) relative to the reference B_1 scan (Ref. DA) were $\rho = 0.92/0.95/0.98$. VFA T_1 correlations using these maps were $\rho = 0.86/0.88/0.96$, much better than without B_1 correction ($\rho = 0.53$). The relative error for each B_1 map (BS/AFI/EPI-DA/Nominal) had 95th percentiles of 5/4/3/13%.

Conclusion: Our findings show that B_1 mapping implemented using product pulse sequences can provide excellent quality B_1 (and VFA T_1) maps, comparable to other custom techniques. This fast whole-brain measurement (~2 min) can serve as an excellent alternative for researchers without access to advanced B_1 pulse sequences.

Level of Evidence: 1

J. MAGN. RESON. IMAGING 2017;00:000–000.

Radiofrequency transmit field (B_1^+) maps, typically termed "B_1 maps" for brevity, are necessary in several quantitative magnetic resonance imaging (MRI) applications, such as specific absorption rate (SAR) estimation, magnetization transfer (MT) imaging, and quantitative T_1 mapping. Electrical properties tomography (EPT) relies on quantitative B_1 maps to calculate the conductivity (σ) and permittivity (ε) of tissue in vivo,[1] and is an essential step in the estimation of local SAR.[2] MT techniques probe the macromolecular content of tissue, and are often used as an index of myelination in diseases such as multiple sclerosis.[3] Unaccounted B_1 inhomogeneity in certain MT experiments can be an important source of error. For example, B_1-correction has been shown to improve the quality of MT ratio (MTR) maps,[4] due to the sensitivity of MTR to the MT preparation RF pulse power. The longitudinal relaxation time (T_1), one of the fundamental quantities in MRI, is an important input for several other data processing pipelines, such as dynamic contrast enhancement (DCE) imaging[5,6] and quantitative MT.[7] Although some whole-brain T_1 mapping methods boast first-order insensitivity to RF field inhomogeneities,[8] others—notably the variable flip angle (VFA) method[9]—are inherently sensitive to inaccuracies in the excitation flip angles (FA). B_1 maps can greatly benefit the accuracy and precision of VFA T_1 maps at high clinical field strengths, (eg, 3T), where large B_1 amplitude variations

View this article online at wileyonlinelibrary.com. DOI: 10.1002/jmri.25692

Received Dec 13, 2016, Accepted for publication Feb 10, 2017.

*Address reprint requests to: M.B., Room WB-325, McConnell Brain Imaging Centre, Montreal Neurological Institute, McGill University, Montreal, Quebec, Canada H3A 2B4. E-mail: mathieu.boudreau2@mail.mcgill.ca

From the [1]Montreal Neurological Institute, McGill University, Montreal, Quebec, Canada; [2]Cerebral Imaging Centre, Douglas Mental Health University Institute, Montreal, Canada; [3]Ecole Polytechnique de Montreal, Montreal, Quebec, Canada; [4]Montreal Heart Institute, University of Montreal, Montreal, Quebec, Canada; [5]Hospital for Sick Children, Toronto, Ontario, Canada; [6]Department of Medical Biophysics, University of Toronto, Ontario, Canada; and [7]Hotchkiss Brain Institute and Department of Radiology, University of Calgary, Calgary, Alberta, Canada

are typical in loaded coils[10] (eg, ± 30% for the human brain). The broad range of B_1 applications highlights the need for accurate B_1 mapping techniques, while also balancing other competing interests such as acquisition speed and ease of implementation, particularly in the context of multi-site studies.

Substantial efforts have been made to develop rapid whole-brain B_1 mapping techniques in the last decade. Previously, conventional B_1 mapping was done using some variations of the double angle (DA) method, which consists of two separate gradient-echo or spin-echo measurements with longitudinal magnetization recovery in which the second measurement is performed with double the excitation pulse flip angle.[11] However, conventional DA requires very long repetition times, and was mostly used for single-slice imaging. Advanced pulse sequences have been developed to accommodate whole-brain B_1 mapping. Two of the most popular techniques are actual flip angle imaging (AFI)[12] and Bloch-Siegert shift (BS) mapping.[13] AFI is a steady-state 3D spoiled gradient echo (SPGR) B_1 mapping method based on a dual-TR acquisition ($TR_2 = N^*TR_1$, where N is typically an integer on the order of 5), and has been shown to be T_1-insensitive for most tissues. BS is a phase-sensitive slice-selective B_1 mapping method using a modified SPGR sequence; a high amplitude off-resonance RF pulse between the excitation and readout events induces a phase-shift proportional to the B_1 amplitude. Currently, an important limitation of these methods is their lack of widespread availability as a standard product sequence on clinical scanners. These pulse sequences are typically implemented on-site, a time-consuming process that require pulse sequence programming expertise, and is susceptible to site-specific implementation issues.

The lack of a readily available whole-brain B_1 mapping pulse sequence is a challenge to many researchers, particularly in the context of multi-center studies, resulting in the omission of B_1 mapping in quantitative imaging protocols that would significantly benefit from its inclusion. One such quantitative MRI method is VFA T_1 mapping, which estimates T_1 by fitting the gradient echo images to a function of flip angles, making it inherently sensitive to B_1 inaccuracies. For example, using a VFA sequence with a 15 msec TR and two flip angles (3° and 20°),[14] an underestimation of the nominal flip angles by 1/5/10/20% results in an overestimation of the fitted T_1 by 2/11/24/57%. Thus, errors in B_1 induce at least twice as large errors in T_1, and the error increases nonlinearly. Notably, DCE imaging protocols that use VFA T_1 mapping often omit B_1 correction,[5,15] even though B_1 maps have been shown to substantially improve the accuracy of DCE.[6,16] Citing the unavailability of advanced B_1 mapping sequences at their site, other researchers have developed techniques to simulate B_1 maps by normalizing the VFA T_1 image[17] using postprocessing image analysis algorithms.[18] However, a systemic bias in B_1 values (of unknown size) could still be present using this type of image analysis approximation, so measuring B_1 directly should improve the accuracy of the T_1 maps.

The purpose of this work was to evaluate the quality of a fast and simple whole-brain B_1 mapping protocol implemented using a standard EPI pulse sequence. An interleaved multislice spin-echo EPI readout standard product pulse sequence was used to map B_1 with the DA method (EPI-DA)[19–21] in a group of healthy human subjects. EPI-DA has not gained as much attraction in comparison to AFI and BS, due to their demonstrated robustness against specific characteristics (eg, large T_1 values, B_0 inhomogeneity) and their compatibility with higher fields systems that use parallel transmit coils. Yet the ease of implementation of EPI-DA or other similar techniques (eg, fast spin-echo DA[22]) may make them a good alternative to advanced B_1 methods, which require custom implementations and pulse sequence programming expertise.

Materials and Methods

All measurements were performed on a 3.0T whole-body MRI scanner (Magnetom TIM TRIO, Siemens, Erlangen, Germany) using a 32-channel phased-array receive-only head coil and whole-body transmit coil.

Measurements

Healthy adult volunteers were scanned in compliance with the guidelines of the Institutional Ethics Committee, and gave written informed consent prior to being scanned for this study. Six healthy adult volunteers were scanned (three females, three males, 29 ± 3 years old). Axial slices were acquired (for 2D measurements) or extracted (from 3D/multislice measurements, with orientations matching the single-slice 2D measurements) parallel to the anterior and posterior commissure (AC-PC) plane, superior to the corpus callosum.

Quantitative analyses of the B_1 and T_1 maps were limited to voxels comprised of white matter (WM), consistent with previous work.[22,23] Two reasons factored into this decision. First, as B_1 maps are typically acquired at low resolution, partial volume effects occur near cortical gray matter (GM) regions and areas adjacent to ventricles. Therefore, there is an insufficient number of voxels that contain pure GM. Second, the partial volume effects in regions containing cerebrospinal fluid (CSF) result in substantially longer mean T_1 values (2–5 sec), so T_1-sensitive artifacts will vary in severity between B_1 methods that have different intrinsic sensitivity to long T_1 and CSF flow. Adequately comparing B_1 methods in GM and CSF is a specialized topic that requires higher resolution and/or longer scan-times, which is beyond the scope of this work.

Whole-brain T_1-weighted magnetization-prepared rapid gradient-echo (MP-RAGE) 3D volumes ($1 \times 1 \times 1\,mm^3$) were acquired: repetition time (TR) = 2300 msec, echo time (TE) = 3.32 msec, inversion time (TI) = 900 msec, iPAT factor = 2 (GRAPPA), bandwidth (BW) = 230 Hz/Px, 5 min 30 sec scan

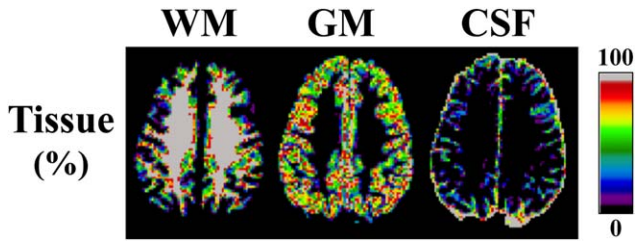

FIGURE 1: Tissue classification maps (black = 0%, gray = 100%) of a healthy subject calculated from INSECT[21] using MP-RAGE T_{1w} data (1 × 1 × 1 mm^3) and resampled to 2 × 2 × 5 mm^3. Tissue percentages were estimated by calculating the ratio of INSECT tissue-classified voxels (1 mm^3) for a given tissue type (WM, GM, CSF) that were located inside the corresponding low-resolution voxels (2 × 2 × 5 mm^3), for which the quantitative maps (B_1, T_1) were acquired.

time. Tissue classification maps (WM, GM, CSF) were obtained via Intensity Normalized Stereotaxic Environment for the Classification of Tissue (INSECT)[24] using the MP-RAGE data with the ICBM-152 atlas. All necessary preprocessing steps (nonuniformity correction, skull-stripping, etc.) were done using the standard pipeline of the MINC Tool Kit (v. 1.9.11, McConnell Brain Imaging Center, Montreal Neurological Institute, Montreal, Canada). Tissue percentage maps (WM, GM, CSF), at the low resolution (2 × 2 × 5 mm^3) for which the quantitative maps (B_1, T_1) were acquired, were estimated by calculating the ratio of high-resolution INSECT tissue-classified voxels (1 mm^3) that had the center of their voxels located within the corresponding 2 × 2 × 5 mm^3 voxels. using a majority voting analysis (75% threshold). Figure 1 shows a tissue classification maps of WM, GM, and CSF for a healthy subject. The classification maps show that for a 2 × 2 × 5 mm^3 resolution, very few voxels consisted of single-tissue GM or CSF, reaffirming our reasoning to exclude these areas in our study. To generate the WM masks for each subject, a >75% binary threshold was applied to the tissue percentage maps; since there can be 20 high-resolution voxels (1 mm^3) that have their centers located in a low-resolution voxels (2 × 2 × 5 mm^3), a >75% threshold represents the case that no more than four non-WM INSECT tissue-classified voxels (out of 20) are located within a voxel of the WM mask. Lastly, note that the WM mask were only used to mask-out non-WM voxels after the B_1 maps were calculated, and are not required to calculate any of the B_1 maps described in the following section.

B_1 Mapping

Three rapid B_1 mapping techniques (Bloch-Siegert shift, BS; actual flip angle imaging, AFI; echo planar imaging double angle, EPI-DA) were acquired with acquisition protocols that matched their original publications values as closely as possible. A single-slice double angle B_1 map was acquired as a reference (Red. DA), as is typical.[13,25] Lastly, a uniform B_1 map of value 1 normalized units (n.u.), noted in short-hand as "Nominal," was generated to represent the case when VFA T_1 values are fitted using the nominal flip angles of its acquisition protocol.

BLOCH-SIEGERT (BS). Single-slice BS B_1 maps[13] were acquired using an in-house-developed pulse sequence: TE/TR = 15/100 msec, excitation flip angle (α) = 25°, field-of-view (FOV) = 25.6 × 17.6 cm^2, 2 × 2 mm^2 in-plane resolution, 128 × 88 matrix (readout/phase), 5 mm slice thickness, 1 slice, 8 msec Fermi Pulse of 500° at ± 4 kHz off-resonance and phase-shift constant K_{BS} = 74.01 rad/G^2, 19 sec scan time.

ACTUAL FLIP ANGLE IMAGING (AFI). AFI B_1 maps were acquired using an in-house-written slab-selective 3D AFI pulse sequence with optimal RF and gradient spoiling[12,26]: TE/TR1/TR2 3.53/20/100 msec, α = 60°, BW = 260 Hz/pixel, FOV = 25.6 × 17.6 × 16.0 cm^3, 2 × 2 × 5 mm^3 resolution, 128 × 88 × 32 matrix (readout/phase/3D), spoiling gradient moment (A_G) = 450 mT·ms/m and RF phase increment (ψ) = 39°, 5 min 38 sec scan time.

EPI DOUBLE ANGLE (EPI-DA). Interleaved multislice spin-echo EPI-DA B_1 maps with whole-brain coverage were acquired using a standard product EPI pulse sequence with a protocol similar to that of Wang et al,[19] except with 180° refocusing pulses (the scanner default for this sequence). Since our sequence used (α, 180°) and (2α, 180°) excitation-refocusing pulses, instead of (α, 2α) and (2α, 4α) in the original article, the equation used to calculate EPI-DA B_1 was[11,22]:

$$B_1 \equiv \frac{\alpha_{corr}}{\alpha} = \frac{\cos^{-1}\left(\frac{I_2}{2I_1}\right)}{\alpha} \quad (1)$$

where α is the nominal flip angle (double for the second measurement), α_{corr} is the true flip angle experienced by the tissue at that voxel location, I_1 and I_2 are the image voxels magnitudes for α and 2α acquisition, respectively. The EPI-DA acquisition protocol was: TE/TR = 46/4000 msec, $\alpha/2\alpha$ = 60°/120°, FOV = 25.6 × 25.6 cm^2, 2 × 2 mm^2 in-plane resolution, 128 × 128 matrix (readout/phase), 5 mm slice thickness, 27 slices, EPI factor = 9 (15 shots of 9 *k*-space readout line acquisitions), echo spacing = 4.18 msec, fat saturation on, BW = 250 Hz/px, 2 min 16 sec scan time. Standard automated shimming was performed as with all other sequences (shim currents adjusted using a 3D phase map); no additional adjustments of the static or gradient fields were necessary.

Fast EPI sequences, such as the widely used single-shot implementations, can be susceptible to a wide range of artifacts that lead to a degradation of image quality. Several strategies are incorporated in this protocol to mitigate these artifacts, while still using a readily available scanner sequence and maintaining rapid overall acquisition. A segmented multishot EPI approach increases the effective BW in the phase-encode direction, which reduces distortion artifacts that are typically prevalent in areas of high B_0 inhomogeneity such as near the sinuses. Blurring is also reduced, due to decreased T_2^* modulation in each acquired echo train. Acquiring the B_1 map at a low in-plane resolution (2 × 2 mm^2) also means smaller readout gradient amplitudes are used, reducing potential eddy current artifacts (eg, ghosting). Other fast imaging techniques, such as fast spin-echo, have also been adapted for whole-brain double angle B_1 mapping.[22] These methods could offer different imaging benefits as alternatives to EPI; however, such a comparison is outside the scope of the present work.

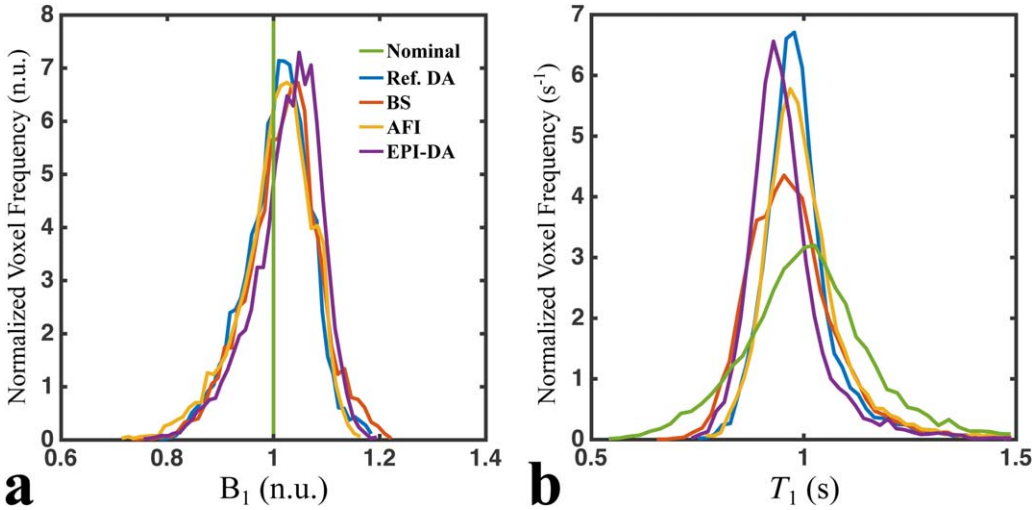

FIGURE 2: Normalized histograms of single-slice unfiltered B_1 (a) and T_1 (b) map values masked for WM in six healthy subjects. The abbreviation "n.u." stands for normalized units.

REFERENCE DOUBLE ANGLE (REF. DA). Single-slice double angle B_1 maps were acquired using a spin-echo sequence as a reference measurement for the other B_1 mapping techniques: TE/TR 12/1550 msec, $\alpha = 60°/120°$, FOV = 25.6 × 17.6 cm^2, 2 × 2 mm^2 in-plane resolution, 128 × 88 matrix (readout/phase), 5 mm slice thickness, 1 slice, slice-selective excitation and 180° refocusing pulses, and BW = 130 Hz/pixel, 4 min 28 sec scan time. The flip angles were chosen to match the EPI-DA sequence. As Ref. DA is the most time costly of all the compared methods (4 min 38 sec), a shorter TR was chosen to reduce the acquisition time of the entire protocol while maintaining sufficient accuracy in WM.[14] The TR is sufficiently long to allow almost complete relaxation of the WM signal, which we are evaluating.

Overall, each pulse sequence had the following effective acquisition time per slice: Ref. DA: 4 min 38 sec/slice, BS: 19 sec/slice, AFI: 11 sec/slice (3D measurement), EPI-DA: 5 sec/slice (interleaved multislice sequence produced 27 slices in 68 sec per flip angle acquisition).

T_1 Mapping

VFA is a widely used T_1 mapping technique; spoiled gradient echo images are acquired using multiple (usually 2–5) excitation flip angles, each using the same TR. VFA T_1 maps were acquired using a standard product spoiled 3D gradient echo pulse sequence: 2 × 2 × 5 mm^3 resolution, 128 × 88 × 32 matrix (readout/phase/3D), TE/TR 2.89/15 msec, $\alpha = 3°/20°$, BW = 390 Hz/pixel, default manufacturer slab-selection and RF spoiling modes, 1 min 28 sec scan time.

Data Analysis

B_1 and T_1 maps were processed from the MRI data using custom MATLAB code (MathWorks, Natick, MA). Each B_1 map was used to scale the VFA nominal flip angles voxelwise prior to fitting for T_1. T_1 maps were estimated from linear least square fitting to the SPGR equation.[14]

The B_1 amplitude is expected to be a smooth slowly varying function, particularly in the brain.[18] As such, B_1 maps are commonly filtered to reduce noise and minor artifacts.[12,25] Subjective assessment of the images was performed by two of the coauthors (coauthors #3 and #6) who were blinded to the acquisition method used for each dataset. They provided a brief subjective evaluation of any artifacts they observed. A consensus opinion was then formed via discussion between all coauthors. In addition to comparing unfiltered (raw) B_1 maps (as well as in the VFA T_1 analysis), we repeated the data analysis using filtered B_1 maps. Single-slice B_1 maps were filtered (prior to WM masking) using the MATLAB function *roifilt2* and skull-stripped brain masks (all tissues). A Gaussian kernel (*fspecial*) was used with a full-width-half-maximum of 10 × 10 mm^2 (sigma = 4.2466) and a 7 × 7 voxel kernel matrix.

The voxelwise WM B_1 and T_1 data for each method (Ref. DA, BS, AFI, EPI-DA) and the nominal flip angle case (Nominal) were pooled together (all subjects) for data analysis. Histograms of the unfiltered B_1 maps and accompanying fitted T_1 values were calculated to investigate the presence of potential systemic biases or spreading between methods.[14,22] Linear regression analysis of B_1 and T_1 (Pearson correlation and linear fit values) was performed for each B_1 method relative to the Ref. DA B_1 values. The linear regression analysis was performed using both the unfiltered and the Gaussian filtered B_1 data.

Results

Pooled-subject histograms of unfiltered B_1 map values from WM regions are shown in Fig. 2a. There is an overlap between the different B_1 histograms; the differences in statistical modes (ΔMode) for each method relative to Ref. DA were 3.6/1.5/3.8% (BS/AFI/EPI-DA). EPI-DA is the only method for which a small B_1 histogram shift is qualitatively observable, which suggests the presence of a small systemic bias. The unfiltered B_1 maps for a single subject are shown in Fig. 3b, along with their accompanying acquisition images in Fig. 3a. The signal-to-noise ratio (SNR) in a region-of-interest of WM was estimated across all subjects to be 240 ± 45 for Ref. DA, 98 ± 11 for BS, 170 ± 35 for AFI, and 130 ± 30 for EPI-DA. Linear regression statistics

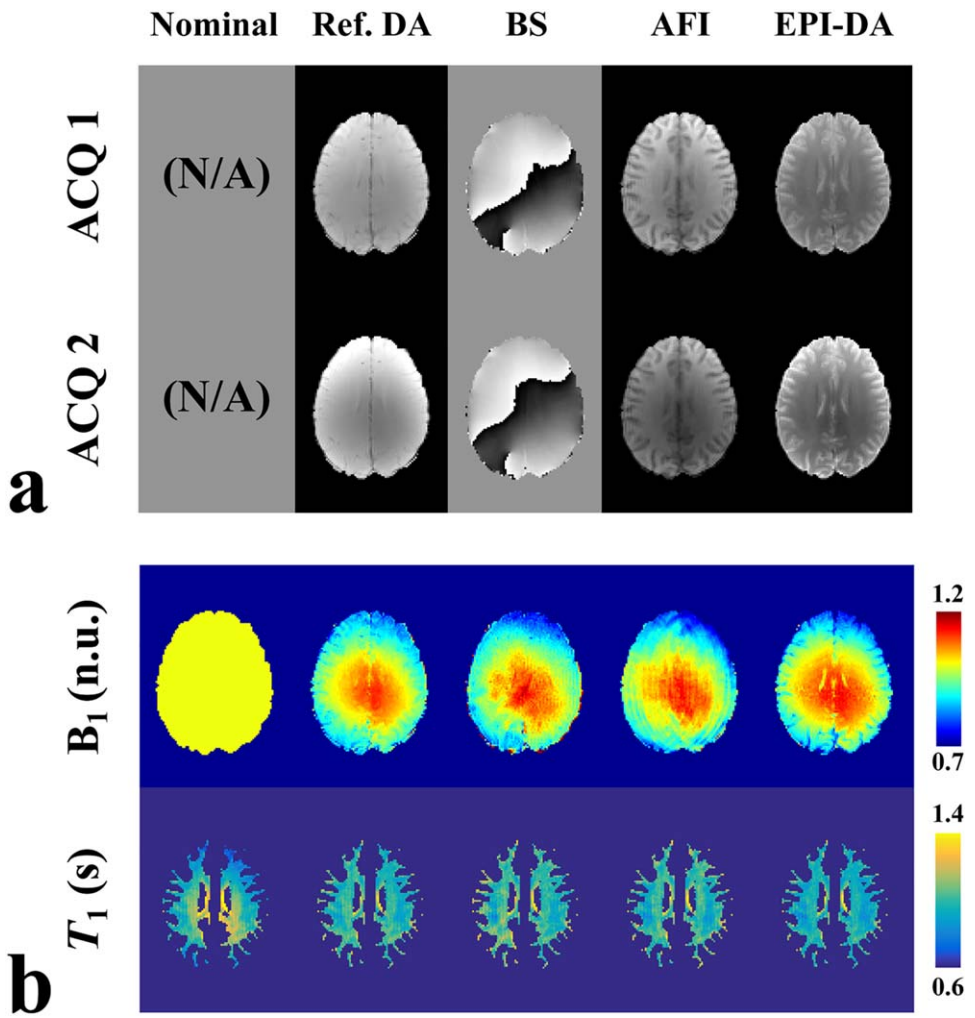

FIGURE 3: a: Acquisition images for each acquired B_1 method: Ref. DA (reference single-slice double angle), AFI (actual flip angle imaging), BS (Bloch-Siegert shift), and EPI-DA (double-angle using an interleaved multislice EPI acquisition). b: Unfiltered single-slice B_1 maps, and corresponding WM-masked VFA T_1 maps fitted using flip-angles scaled voxelwise using each B_1 map. The "Nominal" column represents VFA T_1 fitting using no B_1 correction ($B_1 = 1$ n.u.).

computed using the pooled voxelwise data for each unfiltered B_1 map (BS, AFI, EPI-DA) relative to the Ref. DA measurement is presented in Table 1. EPI-DA had the highest Pearson correlation coefficient relative to Ref. DA ($\rho = 0.96$) and a near-unity slope ($\beta = 0.99$); the BS B_1 maps had the lowest correlation out of the three ($\rho = 0.88$).

TABLE 1. Linear Regression Analysis of the Pooled WM-Masked B_1 and T_1 Values (Six Subjects) for Each Rapid B_1 Method Relative to the Ref. DA Method

				Unfiltered B_1 maps			Gaussian filtered B_1 maps		
		Ref. DA	Nominal	BS	AFI	EPI-DA	BS	AFI	EPI-DA
B_1	Pearson ρ	---------	N/A	0.88	0.92	0.96	0.92	0.95	0.98
	Slope β	---------	N/A	0.97	1.01	0.99	0.96	0.99	1.01
	Intercept y_0	---------	N/A	0.04	-0.01	0.03	0.05	0.00	0.01
T_1	Pearson ρ	---------	0.53	0.79	0.81	0.92	0.86	0.88	0.96
	Slope β	---------	0.95	0.99	0.89	0.94	0.97	0.92	0.98
	Intercept y_0	---------	0.07	0.00	0.12	0.02	0.00	0.09	-0.02

The B_1 methods listed are abbreviated as follows: reference double angle method (Ref. DA), Bloch-Siegert shift (BS), actual flip angle imaging (AFI), and double angle with EPI readout (EPI-DA). The analysis was done using unfiltered B_1 maps, as well as Gaussian filtered B_1 maps (skull-stripped for filtering, and subsequently masked for WM).

TABLE 2. Mean and Standard Deviations of Voxelwise Percent Differences (%) of B_1 and T_1 Values in WM Relative to the Ref. DA Method for All Subjects

Mean ± SD voxelwise percent differences (%) in white matter						
	Subject #	**Ref. DA**	**Nominal**	**BS**	**AFI**	**EPI-DA**
B_1	1	---------	N/A	0.31 ± 3.47	0.47 ± 1.83	1.67 ± 1.43
	2	---------	N/A	3.34 ± 2.46	−1.46 ± 2.40	2.41 ± 1.32
	3	---------	N/A	0.95 ± 2.24	−0.44 ± 2.22	1.87 ± 1.49
	4	---------	N/A	1.57 ± 2.43	−1.28 ± 3.12	0.15 ± 1.66
	5	---------	N/A	−0.01 ± 3.61	0.63 ± 2.09	2.37 ± 1.45
	6	---------	N/A	2.07 ± -0.69	−0.69 ± 3.07	1.76 ± 2.08
T_1	1	---------	−2.11 ± 12.12	−0.30 ± 6.83	−0.85 ± 3.78	−3.27 ± 2.70
	2	---------	2.86 ± 10.96	−6.25 ± 4.67	3.17 ± 5.07	−4.64 ± 2.50
	3	---------	0.46 ± 10.64	2.10 ± 4.69	1.03 ± 4.66	−3.72 ± 2.59
	4	---------	10.27 ± 14.19	−3.01 ± 4.84	2.69 ± 6.60	−0.54 ± 2.60
	5	---------	3.40 ± 11.01	0.32 ± 7.02	−1.09 ± 4.16	−4.53 ± 2.72
	6	---------	−2.70 ± 10.54	−3.86 ± 4.93	1.56 ± 6.70	−3.39 ± 4.36

Unfiltered B_1 maps were used for both the voxel-wise percent difference calculations, and VFA T_1 flip angle correction. "Nominal" is a B_1 map with all voxels equal to 1 n.u.

Table 2 lists the mean and SD of voxelwise differences (%) in WM for each B_1 method relative to Ref. DA. Overall, EPI-DA had a lower voxelwise percent differences SD than other methods for all subjects, except subject #6, where BS had a lower value.

The pooled-subject histogram analysis of WM T_1 values is shown in Fig. 2b. Each measured B_1 map resulted in narrower WM T_1 histograms than for the Nominal case. The differences in statistical modes (ΔMode) for WM T_1 between Ref. DA and BS/AFI/EPI-DA/Nominal were 2.5/1.0/5.0/5.0%, respectively. The width of the WM T_1 distributions had more relative variation between methods than observed for the B_1 histograms. EPI-DA had the largest ΔMode value (5%), but did not experience noticeable broadening relative to Ref. DA. However, BS clearly did suffer from broadening, yet much less severe than the Nominal case. The small reduction in EPI-DA WM T_1 histogram statistical mode (Fig. 2b) is attributed to the small increase in the corresponding B_1 histogram statistical mode (Fig. 2a). T_1 correlations were lower relative to their respective B_1 correlations, which was to be expected due to the B_1-sensitivity of the VFA technique. Overall, EPI-DA T_1 maps had the highest correlation relative to Ref. DA ($\rho = 0.92$), which was substantially better than for the Nominal case ($\rho = 0.53$). WM-masked T_1 maps are shown for a single subject in Fig. 3. Large overestimations of T_1 at the center of the slice are clearly seen for the Nominal case, unlike those using each measured B_1 map.

Artifacts in the unfiltered B_1 maps differ between methods due to their differing acquisition pulse sequences (Fig. 3b). The sulci are visible in the B_1 maps of both DA methods (Ref. DA and EPI-DA), unlike BS and AFI. In the ventricles, lower B_1 values are present for Ref. DA and EPI-DA relative to the other methods (Figs. 3b, 5). An open-ended fringe line (pole) was present in the Bloch-Siegert phase maps (Fig. 3a), due to out-of-phase multichannel image recombination,[27] and may have caused some inhomogeneity in the Bloch-Siegert B_1 maps in the posterior left hemisphere (Fig. 3b). This phase image artifact was present in all subjects. For BS, the inhomogeneities near the phase

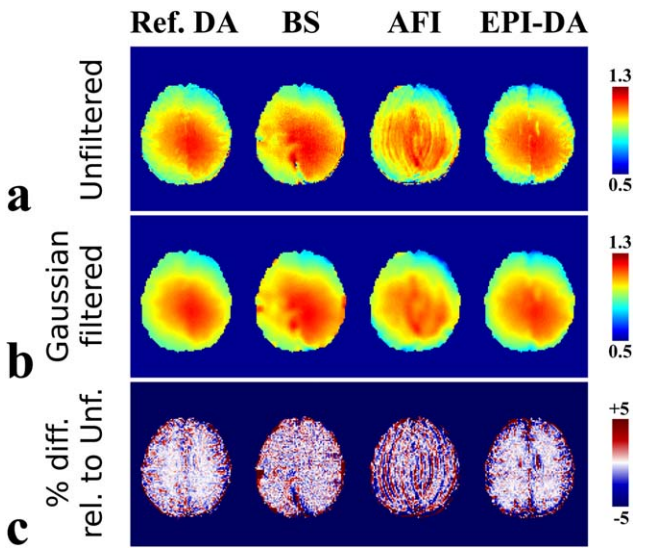

FIGURE 4: Unfiltered (a) and Gaussian filtered (b) B_1 maps of a single subject. (c) Relative differences between unfiltered and filtered maps shown as percent difference maps.

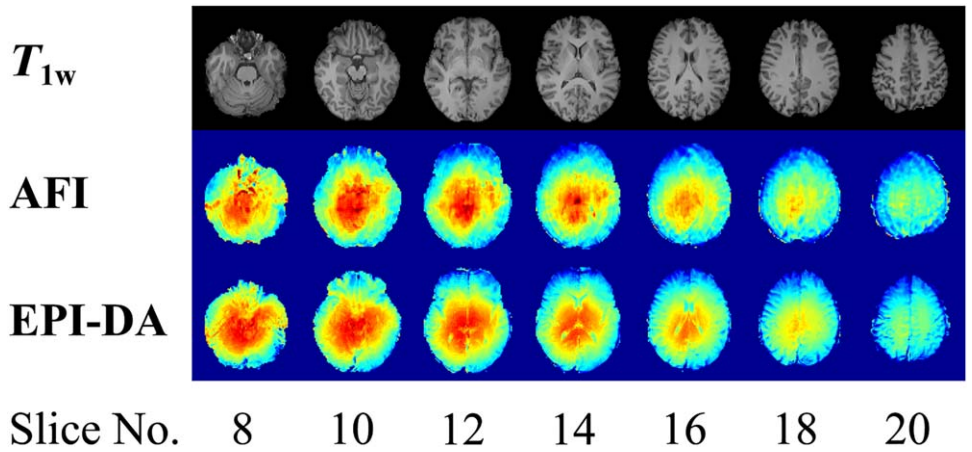

FIGURE 5: Whole-brain coverage of axial MP-RAGE T_{1w} slices, unfiltered AFI B_1 maps, and unfiltered EPI-DA B_1 maps in one subject.

pole along with noisier B_1 maps were likely contributing factors in the broadening of the WM T_1 distribution (Fig. 2b). A ringing artifact affected the AFI B_1 maps (Fig. 3b), although it is not easily seen in the raw AFI acquisition images themselves (Fig. 3a). However, by carefully adjusting the window/level (not shown), a small ringing artifact is present in both AFI MRI images. We observed this ringing in both the raw data and B_1 maps of all subjects. If the ringing between both images is out-of-phase, the resulting B_1 artifact may be amplified due to the nature of the AFI calculation, which requires a division of the two images. The original AFI work only presents their B_1 maps postfiltering ($8 \times 8 \times 16\,mm^3$ median filter); however, ringing can also be seen in their axial and coronal TR1 images (fig. 10a in Ref. 12). Overall, these artifacts and noise in the unfiltered B_1 maps likely contributed to lower correlations of B_1 and T_1 relative to the reference maps.

The unfiltered and Gaussian filtered B_1 maps are shown for a subject in Fig. 4a,b, and the relative difference (%) between the two is shown in Fig. 4c. The Gaussian filter was effective at reducing noise in the maps, as well as in attenuating minor artifacts (eg, sulci in DA maps, "ringing" in AFI). The correlations and linear regression analysis of B_1 (and VFA T_1) relative to the reference (Ref. DA) were recalculated using the filtered B_1 maps (Table 1). The correlations improved postfiltering; for BS/AFI/EPI-DA, B_1 correlations (ρ) were 0.92/0.95/0.98, and for T_1 they were 0.86/0.88/0.96. The 95th percentiles of the absolute relative differences between the reference B_1 map and BS/AFI/EPI-DA (in WM) were equal or lower than 5% (5/4/3%, respectively), while the nominal flip-angle case had a relative difference (to Ref. DA) 95th percentile of 13%.

The raw images used to calculate an EPI-DA B_1 map for a subject are shown in Fig. 3a. The image quality of the EPI images is comparable to the Ref. DA method, and no observable distortions or ghosting were present in the brain for either the acquisition images or the B_1 map. This observation was consistent in all subjects for the slice used in the data analysis. In addition to the single-slice measurements, two of the B_1 mapping protocols were acquired with whole-brain coverage (AFI and EPI-DA). Axial slices for both B_1 methods are shown in Fig. 5. EPI-DA B_1 maps throughout the brain were free of severe susceptibility-induced distortions. However, the ventricles can be clearly identified in the EPI-DA maps (lower values) unlike for AFI, as AFI is well known to be very robust for a wide range of T_1 values.[12]

Discussion

Our findings demonstrate that B_1 mapping implemented using a standard product EPI pulse sequence (EPI-DA) can provide quality whole-brain B_1 maps with a short acquisition time (~2 min). The B_1 maps were comparable or superior in WM to other well-regarded rapid acquisition B_1 methods (AFI and BS) at 3T. Unfiltered B_1 maps correlated with our reference single-slice measurement (Ref. DA), and we observed an improvement in those correlations after applying a Gaussian filter to the images to reduce noise and attenuate small artifacts. Pooled-subject voxelwise B_1 correlation values (relative to Ref. DA) ranged between $0.88 \leq \rho \leq 0.96$ for unfiltered maps, and $0.92 \leq \rho \leq 0.98$ for filtered maps. The 95th percentile of the relative errors of filtered B_1 maps (compared to Ref. DA) were $\leq$ 5%, nearly three times lower than for the nominal flip-angle case (13%). VFA T_1 maps using Gaussian filtered B_1 maps correlated with those using Ref. DA ($0.88 \leq \rho \leq 0.96$,), unlike for the case using uncorrected (nominal) flip-angles ($\rho = 0.53$). The peak of the WM T_1 histograms varied slightly between methods (1 to 5%), much less than the differences reported between different T_1 mapping techniques themselves (20–30%).[14] Our results demonstrate that double angle B_1 mapping using a standard product EPI sequences can produce whole-brain B_1 maps comparable in quality to rapid techniques (eg, AFI and BS) in a clinically

acceptable scan time (~2 min). While our work was based on a multishot EPI protocol,[19] double angle imaging using other fast *k*-space acquisition strategies could also be considered (eg, double angle using a fast spin-echo readout[22]). Implementing standard product pulse sequence protocols for B_1 mapping avoids time-consuming on-site pulse sequence programming (sequences similar to the one used in our study are commonly offered by other manufacturers[19]), improves accessibility of whole-brain B_1 mapping to researchers without access to custom pulse sequences, and could facilitate protocol standardization between sites.

Other groups have also presented comparison studies of existing B_1 methods. Lutti et al[25] optimized and compared the following methods at 3.0T: AFI, a 3D stimulated-echo B_1 mapping method with EPI readouts, a 2D stimulated echo acquisition mode (STEAM) B_1 mapping method, and single-slice DA as a reference. The two stimulated-echo-based methods required additional quantitative pulse sequences for calibration: the 3D stimulated-echo with single-shot EPI B_1 mapping technique used B_0 maps to correct for distortions, and the 2D STEAM method was calibrated against AFI using a separate measurement on a gel phantom to correct for nonlinearities of the slice-selective pulse. Each method demonstrated good reproducibility, and the largest deviation relative to the reference (DA) was observed with the stimulated-echo EPI method (4%), which is in the range of deviation we observed with our standard product EPI-DA pulse sequence (5% relative to Ref. DA for WM). Despite the benefits of these optimized rapid B_1 methods, wide-scale use is limited, as all methods require pulse sequence programming expertise and additional quantitative measurements. Another important source of B_1 inaccuracies, noise, has been characterized for different B_1 methods (Ref. DA, AFI, and BS) using Monte Carlo simulations and phantoms.[28,29] The authors demonstrated that SNRs as low as 50 can be sufficient for accurate flip angle estimation for the range observed in the brain at 3T, and all of the methods compared in our work had SNRs above this threshold in WM.

Optimal flip angles for VFA are in the low FA range (1–30°) due to short TRs required for whole-brain VFA T_1 mapping.[21] All B_1 methods compared in this work used larger flip angles to map the B_1 intensity (Ref. DA and EPI-DA: 60°/120°; AFI: 60°; BS: 25° and 500°), consistent with the published values in the original articles. Thus, RF amplifier nonlinearities could result in inaccurate low FA estimations. RF amplifier nonlinearity can vary substantially between scanner hardware manufacturers, which may lead to a bias of the corrected low flip angles used for VFA.[30] VFA pulse sequence optimization techniques have been proposed to minimize the impact of RF nonlinearity on T_1 mapping.[31] A modified DA B_1 method has also been proposed to map low flip angles accurately,[30] which could possibly be adapted to use fast *k*-space readout acquisition pulse sequences, such as EPI or fast spin-echo.

For the purpose of our study, a simple single-slice DA method measurement was considered to be our "reference" method, as is often the case in B_1 mapping studies. The Ref. DA acquisition is itself sensitive to sources of inaccuracies, as the typical pulse sequence protocols for Ref. DA render the B_1 maps sensitive to long T_1, particularly in voxels containing CSF. The TR used for this pulse sequence was shorter than conventional implementations; however, it was validated against another robust DA method[32] using a TR = 3000 msec and demonstrated very high voxelwise correlation in WM ($\rho = 0.98$, $y = 0.99x + 0.03$). Longer TRs could be used for improved accuracy; however, such a protocol requires 20 + min for a single slice scan,[13] and motion would become an increasing concern with longer TRs. Slice-select RF pulse profiles may also impact B_1 map accuracy, as nonrectangular RF profiles result in a range of flip angles within a slice (and voxel), particularly for large flip angles. Some techniques have been developed to correct for slice profile effects[33]; however, they add additional complexity in postprocessing and require RF pulse waveform information, which may not always be accessible from the scanner. Single-slice DA imaging can mitigate slice profile inaccuracies by using nonselective excitation pulses[32] or refocusing pulses, yet undesired signal from outside the slice can be a problem if incompletely crushed.[34] All B_1 methods compared in this work used pulse sequences that differ greatly in their mechanism and analysis (saturation recovery: DA; steady-state: AFI; phase: BS), yet still produced voxelwise B_1 values highly correlated with the reference measurement (Ref. DA). Each B_1 method, even considering their imperfections, produced much better T_1 maps than for the case of omitting B_1 correction altogether (Nominal).

Smoothing or blurring filters are typically applied to B_1 maps,[12,25,35] as the B_1 variation in the brain is expected to be smooth and spatially slowly varying.[18] There is no well-established consensus on which filter is ideal for B_1 maps. The types of filters used in the literature are numerous: Gaussian convolution, median filters, spline interpolation, etc. In addition, the size of the blurring kernel used varies widely between studies; ranging from 3 mm[12] to 10 mm.[35] Although filtering the B_1 map is often considered a good practice when used in subsequent B_1-correction applications, unfiltered B_1 maps should also be reported when using, developing, or comparing new B_1 methods. B_1 methods are often only compared postblurring,[12,25] thus not all artifacts (or noise level) may be clearly identifiable, only those not fully attenuated by the filters. Unfiltered B_1 maps display valuable information about scanner and pulse sequence artifacts, which is particularly useful when developing or evaluating new methods. For example, even though the ringing artifact in our AFI measurements can be

attenuated in the B_1 maps using filtering methods, it may be preferable to use preprocessing techniques to eliminate the ringing in the acquisition images before the B_1 map is calculated.[36] Although blurring B_1 maps can attenuate local artifacts, it can also spread inaccuracies (eg, ventricles in our EPI-DA maps). If tissue masks are available, specific tissues known to produce inaccurate B_1 values (eg, for the multislice EPI-DA case, cerebrospinal fluid) could be masked, and B_1 values could be interpolated in these regions to approximate the missing values.

The specific scope of this work is limited to applications at clinical field strengths. B_1 mapping at ultrahigh field strengths must be robust against more B_0 inhomogeneity, longer T_1 values, and faces additional hardware challenges, such as parallel transmit.[37] Accelerating B_1 mapping methods using an EPI-based acquisition scheme can be prone to significant susceptibility distortions and signal dropouts at ultrahigh fields.[38] However, Bloch-Siegert at 7T requires additional acceleration techniques like EPI due to its high SAR RF pulses.[39] Supplementary scans (eg, B_0 map) can be used in EPI-based B_1 mapping to correct the distortions,[40] but at the cost of a longer total scan time. Investigating structural characteristics of the cortex is also a topic of great interest in high-field MRI, due to its capability to image at very high resolutions ($\leq 1\,mm^3$). High-resolution VFA T_1 mapping of the cortex must use B_1 maps acquired using a method that has a good robustness against the long T_1 of CSF that neighbors the cortical regions,[41] such as AFI, BS, or other advanced B_1 mapping techniques.

This study had some limitations. The decision to use single-slice B_1 for a reference limited the quantitative comparison between methods to a single slice of the brain. Although using a single-slice DA B_1 map as a reference is common for validating whole-brain methods,[13,25] one solution could be to acquire two more slices in perpendicular planes. Another limitation was that the low resolution of the reference scan restricted the quantitative assessment of B_1 and T_1 values to WM. To quantitatively compare B_1 maps in the cortex, a faster reference acquisition allowing for higher resolution ($\sim 1\,mm^3$) is needed.

In conclusion, we report that B_1 mapping at 3T implemented using standard product pulse sequences (eg, interleaved multislice EPI double angle) can serve as a sufficient alternative to advanced B_1 methods (eg, actual flip angle imaging, Bloch-Siegert), which are not readily available on most MRI systems. The EPI double angle protocol produced whole-brain B_1 maps in a clinically acceptable scan time (~ 2 min), shorter than the AFI and BS's protocols that were compared (although these methods can be further accelerated by implementing fast acquisition strategies, eg, EPI, fast spin-echo, or spiral). All investigated B_1 mapping methods correlated well with a reference measurement, and produced substantially better VFA T_1 maps than in the absence of B_1 correction. The agreement between B_1 maps and resulting T_1 maps were improved by filtering the B_1 maps to reduce noise and minor artifacts. B_1 mapping implemented with standard product pulse sequences can provide an excellent alternative for researchers without custom rapid whole-brain B_1 methods and is much preferred to omitting B_1 correction altogether.

Acknowledgments

Contract grant sponsor: National Sciences and Engineering Research Council of Canada with the Alexander Graham Bell Canada Graduate Scholarships-Doctoral program (to M.B.); Contract grant sponsor: CIHR and Campus Alberta Innovates grants (to G.B.P.)

References

1. Liu J, Zhang X, Schmitter S, Van de Moortele PF, He B. Gradient-based electrical properties tomography (gEPT): A robust method for mapping electrical properties of biological tissues in vivo using magnetic resonance imaging. Magn Reson Med 2015;74:634–646.
2. Katscher U, Voigt T, Findeklee C, Vernickel P, Nehrke K, Dossel O. Determination of electric conductivity and local SAR via B1 mapping. IEEE Trans Med Imaging 2009;28:1365–1374.
3. Schmierer K, Tozer DJ, Scaravilli F, et al. Quantitative magnetization transfer imaging in postmortem multiple sclerosis brain. J Magn Reson Imaging 2007;26:41–51.
4. Ropele S, Filippi M, Valsasina P, et al. Assessment and correction of B1-induced errors in magnetization transfer ratio measurements. Magn Reson Med 2005;53:134–140.
5. Yuan J, Chow SK, Yeung DK, Ahuja AT, King AD. Quantitative evaluation of dual-flip-angle T1 mapping on DCE-MRI kinetic parameter estimation in head and neck. Quant Imaging Med Surg 2012;2:245–253.
6. Sung K, Daniel BL, Hargreaves BA. Transmit B1 + field inhomogeneity and T1 estimation errors in breast DCE-MRI at 3 tesla. J Magn Reson Imaging 2013;38:454–459.
7. Sled JG, Pike GB. Quantitative imaging of magnetization transfer exchange and relaxation properties in vivo using MRI. Magn Reson Med 2001;46:923–931.
8. Marques JP, Kober T, Krueger G, van der Zwaag W, Van de Moortele PF, Gruetter R. MP2RAGE, a self bias-field corrected sequence for improved segmentation and T1-mapping at high field. Neuroimage 2010;49:1271–1281.
9. Gupta RK. New look at method of variable nutation angle for measurement of spin-lattice relaxation-times using Fourier-transform NMR. J Magn Reson 1977;25:231–235.
10. Sled JG, Pike GB. Standing-wave and RF penetration artifacts caused by elliptic geometry: an electrodynamic analysis of MRI. IEEE Trans Med Imaging 1998;17:653–662.
11. Insko EK, Bolinger L. Mapping of the radiofrequency field. J Magn Reson Ser A 1993;103:82–85.
12. Yarnykh VL. Actual flip-angle imaging in the pulsed steady state: a method for rapid three-dimensional mapping of the transmitted radiofrequency field. Magn Reson Med 2007;57:192–200.
13. Sacolick LI, Wiesinger F, Hancu I, Vogel MW. B1 mapping by Bloch-Siegert shift. Magn Reson Med 2010;63:1315–1322.
14. Stikov N, Boudreau M, Levesque IR, Tardif CL, Barral JK, Pike GB. On the accuracy of T1 mapping: searching for common ground. Magn Reson Med 2015;73:514–522.

15. Leppert IR, Narayanan S, Araujo D, et al. Interpreting therapeutic effect in multiple sclerosis via MRI contrast enhancing lesions: now you see them, now you don't. J Neurol 2014;261:809–816.
16. Di Giovanni P, Azlan CA, Ahearn TS, Semple SI, Gilbert FJ, Redpath TW. The accuracy of pharmacokinetic parameter measurement in DCE-MRI of the breast at 3 T. Phys Med Biol 2010;55:121–132.
17. Liberman G, Louzoun Y, Ben Bashat D. T(1) mapping using variable flip angle SPGR data with flip angle correction. J Magn Reson Imaging 2014;40:171–180.
18. Sled JG, Zijdenbos AP, Evans AC. A nonparametric method for automatic correction of intensity nonuniformity in MRI data. IEEE Trans Med Imaging 1998;17:87–97.
19. Wang J, Qiu M, Constable RT. In vivo method for correcting transmit/receive nonuniformities with phased array coils. Magn Reson Med 2005;53:666–674.
20. Wang J, Qiu M, Kim H, Constable RT. T1 measurements incorporating flip angle calibration and correction in vivo. J Magn Reson 2006; 182:283–292.
21. Cheng HL, Wright GA. Rapid high-resolution T(1) mapping by variable flip angles: accurate and precise measurements in the presence of radiofrequency field inhomogeneity. Magn Reson Med 2006;55:566–574.
22. Samson RS, Wheeler-Kingshott CA, Symms MR, Tozer DJ, Tofts PS. A simple correction for B1 field errors in magnetization transfer ratio measurements. Magn Reson Imaging 2006;24:255–263.
23. Stikov N, Campbell JS, Stroh T, et al. In vivo histology of the myelin g-ratio with magnetic resonance imaging. Neuroimage 2015;118:397–405.
24. Collins DL, Zijdenbos A, Baaré WC, Evans A. ANIMAL+INSECT: improved cortical structure segmentation. In: Kuba A, Šáamal M, Todd-Pokropek A, editors. Information processing in medical imaging. Vol. 1613, Lecture Notes in Computer Science. Berlin, Heidelberg: Springer; 1999. p 210–223.
25. Lutti A, Hutton C, Finsterbusch J, Helms G, Weiskopf N. Optimization and validation of methods for mapping of the radiofrequency transmit field at 3T. Magn Reson Med 2010;64:229–238.
26. Yarnykh VL. Optimal radiofrequency and gradient spoiling for improved accuracy of T1 and B1 measurements using fast steady-state techniques. Magn Reson Med 2010;63:1610–1626.
27. Liu T, Wisnieff C, Lou M, Chen W, Spincemaille P, Wang Y. Nonlinear formulation of the magnetic field to source relationship for robust quantitative susceptibility mapping. Magn Reson Med 2013;69:467–476.
28. Morrell GR, Schabel MC. An analysis of the accuracy of magnetic resonance flip angle measurement methods. Phys Med Biol 2010;55: 6157–6174.
29. Park DJ, Bangerter NK, Javed A, Kaggie J, Khalighi MM, Morrell GR. A statistical analysis of the Bloch-Siegert B1 mapping technique. Phys Med Biol 2013;58:5673–5691.
30. Balezeau F, Eliat PA, Cayamo AB, Saint-Jalmes H. Mapping of low flip angles in magnetic resonance. Phys Med Biol 2011;56:6635–6647.
31. Lutti A, Weiskopf N. Optimizing the accuracy of T1 mapping accounting for RF non-linearities and spoiling characteristics in FLASH imaging. In: Proc 21st Annual Meeting ISMRM, Milan; 2014 (abstract 2478).
32. Sled JG, Pike GB. Correction for B1 and B0 variations in quantitative T2 measurements using MRI. Magn Reson Med 2000;43: 589–593.
33. Parker GJ, Barker GJ, Tofts PS. Accurate multislice gradient echo T(1) measurement in the presence of non-ideal RF pulse shape and RF field nonuniformity. Magn Reson Med 2001;45:838–845.
34. Mitsouras D, Mulkern RV, Rybicki FJ. Strategies for inner volume 3D fast spin echo magnetic resonance imaging using nonselective refocusing radio frequency pulses. Med Phys 2006;33:173–186.
35. Helms G, Finsterbusch J, Weiskopf N, Dechent P. Rapid radiofrequency field mapping in vivo using single-shot STEAM MRI. Magn Reson Med 2008;60:739–743.
36. Kellner E, Dhital B, Kiselev VG, Reisert M. Gibbs-ringing artifact removal based on local subvoxel-shifts. Magn Reson Med 2016;76: 1574–1581.
37. Nehrke K, Bornert P. Eigenmode analysis of transmit coil array for tailored B1 mapping. Magn Reson Med 2010;63:754–764.
38. Pohmann R, Scheffler K. A theoretical and experimental comparison of different techniques for B(1) mapping at very high fields. NMR Biomed 2013;26:265–275.
39. Saranathan M, Khalighi MM, Glover GH, Pandit P, Rutt BK. Efficient Bloch-Siegert B1 (+) mapping using spiral and echo-planar readouts. Magn Reson Med 2013;70:1669–1673.
40. Lutti A, Stadler J, Josephs O, et al. Robust and fast whole brain mapping of the RF transmit field B1 at 7T. PLoS One 2012;7:e32379.
41. Lutti A, Dick F, Sereno MI, Weiskopf N. Using high-resolution quantitative mapping of R1 as an index of cortical myelination. NeuroImage 2014;93(Pt 2):176–188.